



Cylinders intruding wet granular beds – experiment and simulation

Jiayi Li, Lijuan Zhang, Kang Han, Shuncheng Lin, Jie Lu, Fengjiao Liu & Jos J. Derksen

To cite this article: Jiayi Li, Lijuan Zhang, Kang Han, Shuncheng Lin, Jie Lu, Fengjiao Liu & Jos J. Derksen (2024) Cylinders intruding wet granular beds – experiment and simulation, Journal of Hydraulic Research, 62:4, 351-364, DOI: [10.1080/00221686.2024.2391459](https://doi.org/10.1080/00221686.2024.2391459)

To link to this article: <https://doi.org/10.1080/00221686.2024.2391459>



Published online: 26 Sep 2024.



Submit your article to this journal [↗](#)





View related articles [↗](#)



View Crossmark data [↗](#)

Cylinders intruding wet granular beds – experiment and simulation

Jiayi Li^a, Lijuan Zhang ^b, Kang Han^c, Shuncheng Lin^d, Jie Lu^e, Fengjiao Liu^f and Jos J. Derksen ^g

^aSchool of Chemistry and Chemical Engineering, Shanghai University of Engineering Science, Shanghai, PR China; ^bSchool of Chemistry and Chemical Engineering, Shanghai University of Engineering Science, Shanghai, PR China; ^cSchool of Chemistry and Chemical Engineering, Shanghai University of Engineering Science, Shanghai, PR China; ^dSchool of Chemistry and Chemical Engineering, Shanghai University of Engineering Science, Shanghai, PR China; ^eSchool of Chemistry and Chemical Engineering, Shanghai University of Engineering Science, Shanghai, PR China; ^fSchool of Chemistry and Chemical Engineering, Shanghai University of Engineering Science, Shanghai, PR China; ^gSchool of Engineering, University of Aberdeen, King's College, Aberdeen, UK

ABSTRACT

Quantitative visualization experiments and numerical simulations on cylindrical “alien” particles penetrating a liquid-saturated granular bed have been performed. The bed consists of mono-sized spheres. In dimensionless terms the bed is characterized by an Archimedes number, an angle of repose that represents friction, and a solids volume fraction. The conditions are such that the fluid flow generated by alien and bed particle motion is laminar. The experiments are well reproducible. The most important experimental observation is deeper penetration of the alien particle for higher liquid viscosities. The spatial resolution of the three-dimensional, time-dependent simulations is such that they resolve the flow around, and the motion of the individual particles. The flow solver is based on the lattice-Boltzmann method. To a certain extent the simulations are able to reproduce the viscosity effect observed experimentally.

ARTICLE HISTORY

Received 26 March 2024
Accepted 6 August 2024
Open for discussion until
1 February 2025

KEYWORDS

Granular bed; immersion depth; interstitial fluid; quantitative visualization; particle-resolved simulation

1. Introduction

There are multiple examples of aquatic sedimentary systems and related practical applications where strong interactions between the granular bed and the fluid flow over and through it are of great importance (Garcia, 2008). In addition to being moved by fluid flow, granular beds also get mobilized and disturbed by intruders. These intruders cover a broad range of applications and have a broad spectrum of sizes and shapes. Examples include vehicles or robots moving over – or getting stuck in – sand beds (Li et al., 2009), projectiles (Nelson et al., 2008), contaminant particles getting buried (Leiser et al., 2021), and piles being driven in soil (Liu et al., 2020). Intruders may also be devices to probe the mechanical properties (e.g. hardness, consistency or effective viscosity) of granular beds (Marston et al., 2012).

Given its relevance and intriguing, sometimes counterintuitive, behaviour (Somfai et al., 2007), there is an extensive body of experimental, computational and theoretical research literature on the behaviour of granular matter. A recent review (Kamrin et al., 2024) discusses the advances in modelling granular media. It is important at this stage to distinguish between dry and wet granular matter, with the present paper exclusively dealing with wet granular matter. Where there are ongoing debates about the role of interstitial air in certain aspects of the behaviour of “dry” granular matter (van der Meer, 2017), there is little doubt that

the presence of liquid in the interstices has significant impact on the way wet granular matter behaves. If granular beds are partly saturated with liquid, interfacial (wetting) phenomena require consideration (e.g. the formation of liquid bridges promoting cohesive forces between particles; Zuñiga et al., 2019). In beds fully saturated with liquid, the liquid's rheology (its viscosity in case of Newtonian fluids) and density are relevant parameters, the effects of which need to be investigated.

The shape of the granules constituting a granular bed is another distinctive factor. In many practical applications, from ground coffee to sand to pellets, the particles are irregularly shaped and have a more or less wide size distribution. Shape determines the way particles stack on top of one another and therefore has an effect on the void fraction and consistency of a granular bed (Donev et al., 2004). In the present paper, however, we will confine ourselves to beds of equally sized spherical particles. This has the advantage of a well-defined and therefore well reproducible experimental system that we see as a base-case upon which to build subsequent work with non-spherical bed particles.

The present paper reports on experiments and particle-resolved simulations of a rigid cylindrical particle (termed “alien” particle) intruding in a liquid saturated granular bed made of rigid spheres all having the same diameter. The incompressible liquid is Newtonian and is thus fully defined by its density and viscosity. The alien particle is released at a certain distance above

the bed, then falls through clear liquid before it hits the bed surface and then penetrates the bed. The main focus of our study is on the role of the interstitial liquid in the penetration process. We conduct quantitative visualization experiments that are able to keep track of the location of the alien particle, also when it is submerged in the granular bed. We vary the liquid viscosity as well as the size and density of the alien particle and use the eventual rest location of the alien particle relative to the bed surface as a major metric for the level of penetration.

Among more, this paper builds upon a previous paper of ours in which particle-resolved numerical simulations of a similar situation were described (J. J. Derksen, 2022). One thing that paper made clear is that input from experiments is essential for an accurate description/simulation of the penetration process. The experimental data not only can serve as validation; they also can serve as an assessment of what the critical parameters of the penetration process are. As an example, the simulations by J. J. Derksen (2022) showed a critical dependency of the penetration depth on the friction between the particles. Experiments are needed – and are reported here – so as to quantify the levels of friction in the wet granular bed. This quantification is subsequently used in the penetration simulations. Another intriguing result of the experiments reported in the current paper was a deeper penetration if the liquid viscosity was increased.

The aim of this paper is to present an experimental data set of the penetration process and to show how these data have been used to develop and inform the simulation procedure.

The paper is organized as follows: in Section 2, we present the experimental set-up and methodology and give an overview of parameter settings and variations. In Section 3 the simulation approach is explained and cases for comparison with experiments are identified.

In Section 4, experimental results are presented with a focus on the effects of the various parameter variations on the alien particle intrusion process. Comparison between experiment and simulation is the subject of Section 5. The final section summarizes the paper, reiterates the main conclusions and identifies future work.

2. Experimental set-up and methods

2.1. Experimental set-up

The schematic layout of the experimental set-up is shown in Figure 1. A container of inner dimensions $100 \times 20 \times 260 \text{ mm}^3$ (width \times depth \times height = $L_x \times L_y \times L_z$) with flat transparent acrylic walls was filled with mono-sized transparent acrylic spheres (diameter $d_b = 2.0 \text{ mm}$, density $\rho_b = 1250 \text{ kg m}^{-3}$) and a Newtonian liquid. The latter is in most cases a glycerol–water mixture, the composition of which has been varied so as to vary the liquid's viscosity; liquid mixture properties are given in Table 1.

The granular bed formed by the spheres has a height of approximately $z_{bs} = 200 \text{ mm}$; the solids volume fraction of the bed is $\phi = 0.55$. To obtain a homogeneous granular bed with reproducible filling fractions we went through the following procedure: prior to each experiment, the granular bed particles were dried thoroughly to achieve a near-zero humidity level; liquid was added followed by stirring and then the container was sealed and left to stand overnight.

In the clear liquid above the bed the alien particle is held fixed in tweezers with its centre on the centreline of the container and with a vertical distance between the centre of the alien particle and the surface of the bed equal to $h = 30 \text{ mm}$. The use of a customized lid and a ruler affixed to the front of the container ensures that the particles are released accurately (within $\pm 0.5 \text{ mm}$) at the centre of the container.

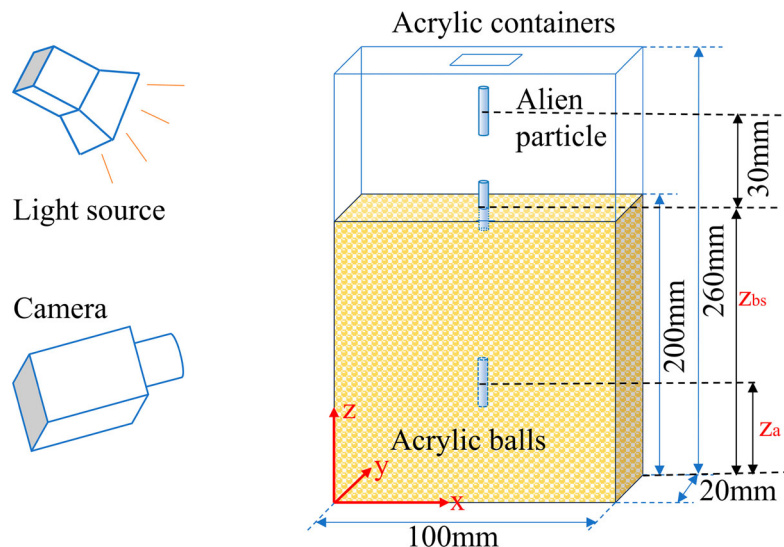


Figure 1. Sketch of the experimental set-up including the coordinate system used throughout the paper.

Table 1. Properties of the interstitial liquids at 24°C; the resting angle is for the granular bed particles (as specified in the text).

Mixture ID	Glycerine-water mixture (volume fraction glycerine)	Density ρ (kg m ⁻³)	Dynamic viscosity η (mPa·s)	Resting angle (°)
#1	0%	997.3	1.16	27.5–27.7
#2	10%	1025	1.72	27.4–27.6
#3	20%	1053	2.12	27.9–28.2
#4	30%	1080	3.14	28.0–28.4
#5	40%	1107	4.28	28.6–28.8
#6	50%	1134	6.89	28.8–29.0
#7	sodium chloride solution	1080	1.56	24.4–24.7

Table 2. Alien particle properties.

Material	Shape	Diameter (mm) d_a	Density (kg m ⁻³) ρ_a	Length (mm) ℓ
Aluminium	cylinder	4	2700	4, 8, 12, 16
Titanium	cylinder	4	4500	4, 8, 12, 16
Stainless steel	cylinder	4	7900	4, 8, 12, 16

After its careful release the alien particle settles towards the bed and then penetrates the bed. The distance between release location and granular bed surface is sufficiently small so that the cylinder does not change its orientation before it hits the bed surface. The process is filmed with a digital camera at a rate of 100 frames per second (fps). Headlight illumination was used to generate a clear view of the alien particle. Given the relatively small size of the bed in the depth (y) direction ($L_y = 20 \text{ mm} = 10 \times d_b$) and the transparency of the bed particles, we are able to see the alien particle (albeit a bit blurred and deformed) after it has penetrated the bed.

A total of 12 different cylindrical particles have been used (Table 2). All cylinders have a diameter of $d_a = 4 \text{ mm}$. Their length ℓ has been varied between 1 and 4 times d_a and their density between $\rho_a = 2700 \text{ kg m}^{-3}$ (aluminium) and 7900 kg m^{-3} (steel).

2.2. Visualization and image analysis

After data collection, the video was split into a series of individual frames; examples of which are given in

Figure 2. Each frame was then analysed and processed by Matlab-based software that first subtracts the background, then applies a threshold to identify the object (i.e. the cylinder) in the image frame and then draws a tight border around it. From this border we derive the xz location of the centre of mass of the cylinder. The main result then is a time series of the vertical (z) location of the centre of mass of the alien particle. As can be seen in Figure 2, once the alien particle has entered the granular bed its image gets blurred by the bed particles in front of it. However, the Matlab programme is still able to identify the alien particle and determine its centre of mass, although with a somewhat increased uncertainty. The uncertainty in the z -location of the centre of mass of the alien particle was analysed and estimated at 0.5 mm in the clear liquid and 1 mm in the granular bed, this corresponds to $0.25d_b$ and $0.5d_b$ respectively.

Figure 3 shows examples of time series of the vertical location of an alien particle; we see an initial acceleration when the particle starts moving through the clear liquid under the influence of gravity and then a deceleration when the particle enters the bed. The three repetitions for the same conditions give an idea of the reproducibility of the experiment. Note that in Figures 2 and 3 we have made time t dimensionless according to tv/d_b^2 with ν the kinematic viscosity of the liquid. This helps us in the rest of the paper to compare the settling process for particles moving through different liquids.

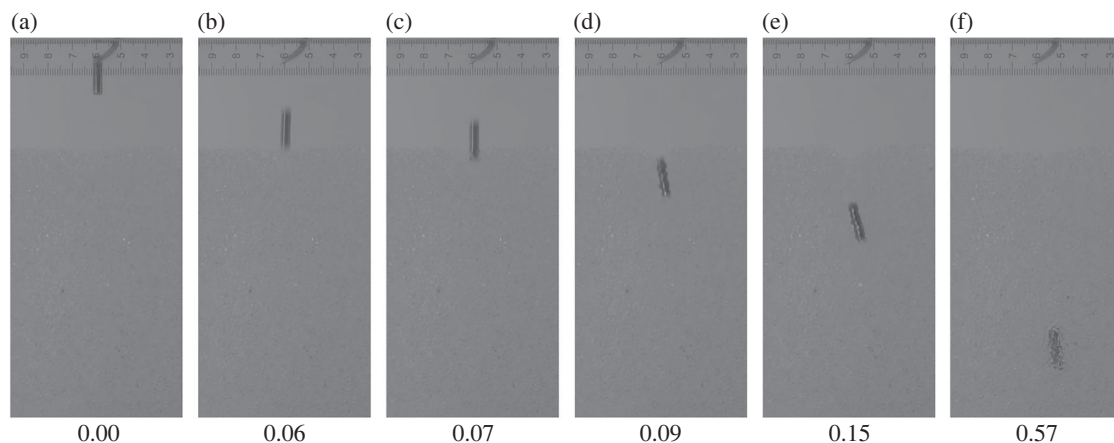


Figure 2. A sequence of snapshots representing the penetration process of a stainless steel cylinder with a diameter of $d_a = 4 \text{ mm}$ and a length of $\ell = 16 \text{ mm}$ into a granular bed with liquid viscosity of $\eta = 3.14 \text{ mPa s}$ (mixture #4; Table 1). Dimensionless time tv/d_b^2 has been indicated for each frame.

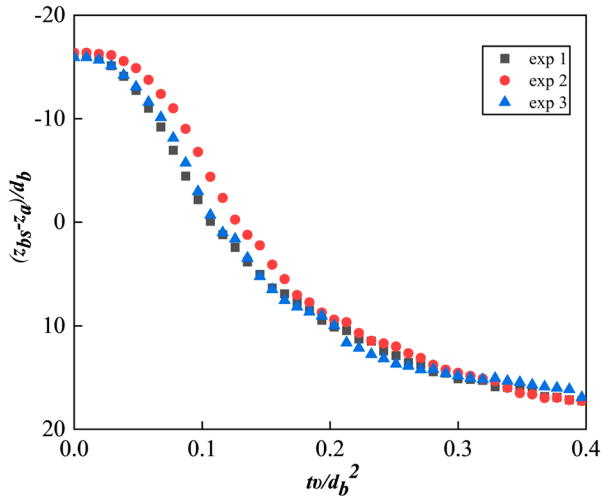


Figure 3. Sample alien particle vertical location (z_a) relative to the bed surface level (z_{b_s}) time series with the same experiment repeated three times. The alien particle is a titanium cylinder of $d_a = 4$ mm diameter and $\ell = 16$ mm length, the liquid is mixture #5 (Table 1).

Table 3. Immersion depth of a $d_a = 4$ mm diameter, $\ell = 16$ mm long stainless steel cylinder settling in a vertical manner into a bed of particles containing liquid mixture #4.

	Immersion depth (mm)	Average value (mm)	Standard deviation (mm)
Experiments	71.5 74.8 71.2	72.5	2.0

An important experimental metric is the penetration depth of the alien particle which can be derived from the eventual z -location of the centre of mass of the alien particle. Each experiment was repeated several times (as shown in Figure 3). The experiment achieved good reproducibility as can be evidenced from Table 3 that shows the penetration depths for one specific case that were within 5%. The error bars that we show in subsequent results for penetration depth are the standard deviations of repeated experiments.

2.3. Angle of repose experiments

In order to characterize the friction between the bed particles, the angle of repose was measured in liquids of different viscosities (these are the liquid mixtures also used in the settling experiments; Table 1) in a closed container that has the same depth ($L_y = 10 d_b$) and was made of the same material as the container used in the settling experiments.

First the particles and the liquid were shaken, after which the container was slowly rotated from an inclined to a vertical position. The eventual angle formed by the surface of the particles with the horizontal is the angle of repose; see Figure 4 for sample measurements. These measured angles of repose are included in Table 1. It can be seen that the angle of repose hardly depends on the liquid's viscosity. The exception is Mixture #7; in

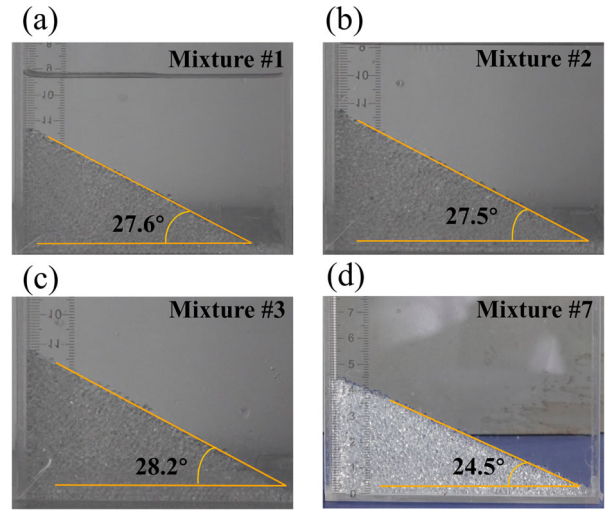


Figure 4. Sample measurements of the rest angle with the same bed particles immersed in different liquid mixtures (Table 1) as indicated per panel. The uncertainty of the rest angle measurement is estimated as $\pm 0.2^\circ$.

this liquid the angle is smaller by $\sim 3^\circ$ compared to the other angles, hinting at slightly reduced friction in this solid–liquid system.

2.4. Overview of experimental cases studied

In the experimental campaign we have varied (1) the liquid properties, most importantly its viscosity (Table 1); (2) the density of the cylindrical (alien) particles; (3) the length of the cylindrical (alien) particles (Table 2); and (4) the orientation (vertical and horizontal) with which the cylinders approach the granular bed. The parameters that have *not* been changed are those of the bed particles, the diameter of the cylindrical (alien particles), the dimensions of the settling container and the starting position (relative to the granular bed surface) of the alien particle. A comprehensive set of dimensionless numbers characterizes the experimental cases; it is listed in Table 4.

3. Simulation procedure and set-up

3.1. Simulation procedure

The simulation procedure that has been followed is the same as described in a recent paper of ours on a similar topic (J. J. Derksen, 2022). The procedure has been detailed in that paper and in the references in that paper. In this section we give a brief summary of the numerical method so as to show its underlying assumptions and approximations.

The flow of the Newtonian liquid is solved by a lattice-Boltzmann (LB) method (Krüger et al., 2017) with the specific numerical scheme due to Eggels and Somers (1995). In this scheme, three-dimensional space is discretized by a uniform lattice of cubic cells with side length Δ , with the flow variables computed at each

Table 4. Definitions and values (or value ranges) of dimensionless numbers derived from experimental conditions.

Dimensionless number	Expression	Value or range
Archimedes number of granular bed	$Ar_b = (\gamma - 1)gd_b^3/\nu^2$	2.2×10^2 to 1.5×10^4
Bed particle density over liquid density	$\gamma = \rho_b/\rho$	1.10 to 1.25
Alien particle density over liquid density	$\gamma_a = \rho_a/\rho$	2.5 to 7.3
Alien particle diameter over bed particle diameter	d_a/d_b	2.0
Length over diameter of alien particle	ℓ/d_a	1.0 to 4.0
Solids volume fraction of the bed	ϕ	0.55
Container aspect ratios	$L_x/d_b, L_y/d_b, L_z/d_b$	50, 10, 130
Granular bed height	z_{bs}/d_b	100
Release height of the alien particle	h/d_b	15
Resting angle	θ	25° to 29°

cell centre. The primary variables of the method are velocity distribution functions. From the distribution functions more common flow variables such as velocity, density and pressure can be derived. The flow system is advanced in time in an explicit manner with a time step Δt .

The particles in the system (one alien particle and of the order of a few thousand granular bed particles) are incorporated by an immersed boundary method (ten Cate et al., 2002). The dimensions of the particles are at least one order of magnitude larger than Δ , so that the lattice is able to resolve the flow around individual particles. The surfaces of each particle are represented by (off-lattice) marker points with a nearest neighbour spacing of approximately 0.5Δ . At these marker points we impose the no-slip condition: the liquid velocity at the marker point is interpolated from the velocity at the surrounding lattice points. This interpolated liquid velocity is compared to the (known) solid surface velocity and any mismatch is negated by exerting a local force on the fluid. The result is that at the marker points the liquid velocity and solid surface velocity are approximately the same and thus no-slip is satisfied. If the force distribution is integrated over each particle surface, we obtain the hydrodynamic force and torque exerted on the particle that we subsequently use to update particle velocity (linear and angular) and location (again linear and angular).

Linear particle dynamics is governed by Newton's second law; rotational dynamics by Euler's equations of motion (Goldstein et al., 2002). The forces involved are hydrodynamic forces, net gravity and close-range interaction forces that include contact forces (these will be discussed below). The torques are due to hydrodynamics and close range interactions. The time step used for updating the particle dynamics is the same Δt

as used for the LB flow updates. Particle orientation calculations use quaternions (Kuipers, 2020).

Identification of close proximity and contact between particles also makes use of marker points at the surface of each particle. Close range interaction forces are activated when the distance between two marker points, each on a different particle, falls below a certain threshold. We distinguish between two types of close-range interaction forces: contact forces and lubrication forces. Lubrication forces are to compensate for a lack of resolution of the flow simulation. When the distance between two particle surfaces falls below Δ , the lattice is not able to properly represent the flow in the gap between the two particles. Based on the relative velocity and the distance between the particle surfaces we then calculate radial and tangential lubrication forces and add those to the other forces exerted on the two particles involved. Expressions for these forces have been detailed in J. J. Derksen (2022). Contact forces become active when two particles touch. Then radial and tangential spring forces are activated. This procedure is also described in J. J. Derksen (2022).

3.2. Set-up of the simulations

The spatial resolution of the simulations was such that the diameter of the granular bed particles spanned 16 grid spacings: $d_b/\Delta = 16$. Past experience (ten Cate et al., 2002) indicates that this is sufficient resolution at the moderate Reynolds numbers as encountered in the experiments. However, with this resolution it is not practical to have a computational system of the same size and the same number of bed particles as in the experiment. Therefore the domains in the simulations are smaller than in the experiments. The experimental granular bed contains approximately 5×10^4 particles. It would be possible to set up a simulation of this size on a high-end computer server; it would, however, take up too much computing time, given our desire to study the effects of input parameter variation and therefore the need to run a significant number of simulations. We consider it important to have the depth of the simulated bed (L_y) the same as in the experiment given that $L_y/d_b = 10$, which means that there is relatively close proximity between the front and the back wall and the intruding alien particle leading to wall effects. The bed needs to be sufficiently deep so that the intruder will stay away from the bottom and sufficiently wide so as to have limited influence of side walls. In the simulations we have checked the sensitivity of both L_x/d_b and L_z/d_b while fixing L_y/d_b to 10.

The walls of the container act as no-slip boundaries for the liquid, except for the top wall where a free-slip condition is applied. The particles interact with the container walls in the same way as they interact with other particles, i.e. through lubrication and contact forces, that each have a normal and a tangential component.

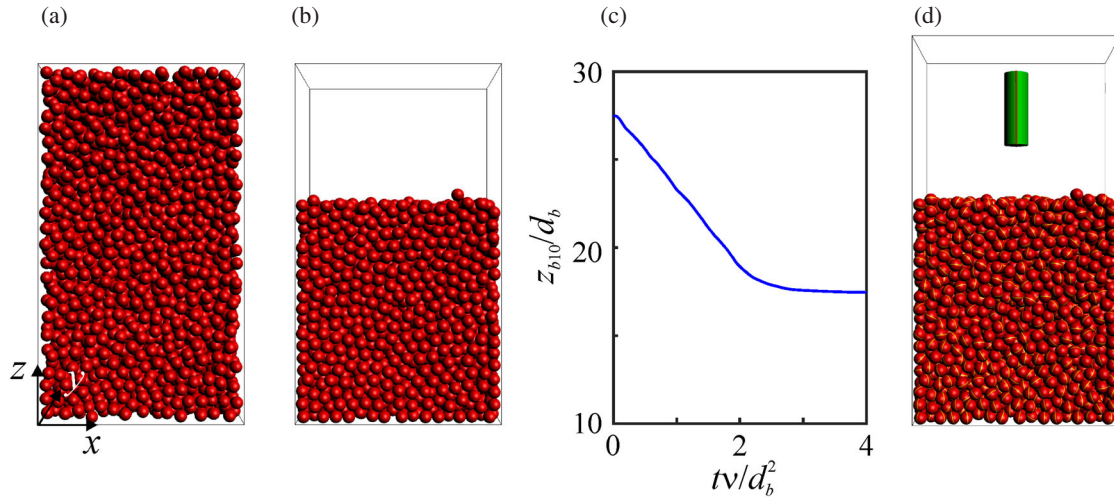


Figure 5. Creation of the granular bed in simulations: (a) initial assembly of non-overlapping bed particles; (b) after settling; (c) time series of the average z -location of the top 10 bed particles (z_{b10}); (d) initial state of the intrusion simulation. Bed Archimedes number: $Ar_b = 1.46 \cdot 10^3$; $L_x = 16d_b$, $L_y = 10d_b$, $H = 28d_b$.

The simulations focus on the comparison between intrusion into two granular beds that consist of the same bed particles but contain two different liquid mixtures. The two mixtures have the same density $\rho = 1080 \text{ kg m}^{-3}$ but different viscosity: $\eta = 3.14 \text{ mPa s}$ and $\eta = 1.56 \text{ mPa s}$; these are mixtures #4 and #7 (Table 1), respectively. These two granular beds have Archimedes numbers $Ar_b = (\gamma - 1)gd_b^3/\nu^2$ of 1.46×10^3 and 5.95×10^3 respectively. In the expression for Ar_b , $\gamma = \rho_b/\rho$, $\nu = \eta/\rho$ and g is gravitational acceleration.

Each simulation consists of two stages: (1) creation of the granular bed; (2) the intrusion process. In Stage 1 we randomly place the spherical bed particles in a non-overlapping way in a domain with size $L_x \times L_y \times H$ with L_x and L_y the size of the eventual intrusion simulation domain in x and y direction and H a height such that the required number of bed particles can be accommodated (Figure 5a). Note that H is larger (by approximately a factor of 2) than the eventual bed height given that randomly placing non-overlapping equally sized spheres can only be done for solids volume fractions up to 0.3 (Torquato et al., 2000). To this domain liquid is added and then we let the particles settle through the liquid under gravity (see the time series of the bed height in Figure 5c). This eventually results in a loosely packed granular bed with a solids volume fraction ϕ in the range 0.53 to 0.54. This value slightly depends on the size of the domain given ordering effects near the bounding walls (e.g. Figure 5b) and is marginally smaller than the experimental value of 0.55 as a result of the smaller size of the numerical beds. After the bed has been formed, we place the alien particle with the desired orientation and location above the bed and, by releasing the alien particle, start the intrusion stage (Stage 2) of the simulation (Figure 5d).

Close-range force interaction expressions contain a number of parameters (J. J. Derksen, 2019). The settings

Table 5. Simulation settings in dimensionless form.

Dimensionless setting	Value
Spatial resolution d_b/Δ	16
Temporal resolution $\sqrt{d_b/g}/\Delta t$	400
Dry friction coefficient μ	0.45
Restitution coefficient e	1.0
Activation distance spring force δ_s/d_b	5×10^{-4}
Spring stiffness $k\delta_s/(g(\rho_b - \rho)\frac{\pi}{6}d_b^3)$	50
Activation distance lubrication force δ_l/d_b	0.0625
CFL number $ \mathbf{u} \Delta/\Delta t$	< 0.1

for these as used in this paper are given in dimensionless form in Table 5. An important parameter is the dry friction coefficient μ . In a previous paper on a similar topic (J. J. Derksen, 2022) it was shown that the penetration process is very sensitive to μ . In the current paper we use the experimental angle of repose results (Figure 4) to select an appropriate dry friction coefficient for the simulations. For this we have set up a series of separate simulations that probe the angle of repose as a function of μ , where the same μ is assumed for particle–particle friction and for particle–wall friction. We start with a settled, loosely packed bed of particles in Newtonian liquid on the bottom of a rectangular container. For the angle of repose simulations we make sure the depth of the container is the same as in the experiments: $L_y = 10d_b$. Using the same Cartesian coordinate system as for the penetration study, the angle-of-repose simulations are then started by slowly rotating the direction of gravity from negative z to positive x , which physically means rotating the container over 90° . This rotation takes $10^5 \Delta t$; in dimensionless terms $10^5 \Delta t \nu/d_b^2 = 2.7$; in physical terms $t = 2.7d_b^2/\nu = 3.7 \text{ s}$ (for mixture #4). At the end of the rotation we continue the simulation until the particles have ceased moving. The corresponding particle configurations are shown in Figure 6 for a range of friction coefficients and for two Archimedes numbers, that is for two liquid viscosities. As in the experiment,

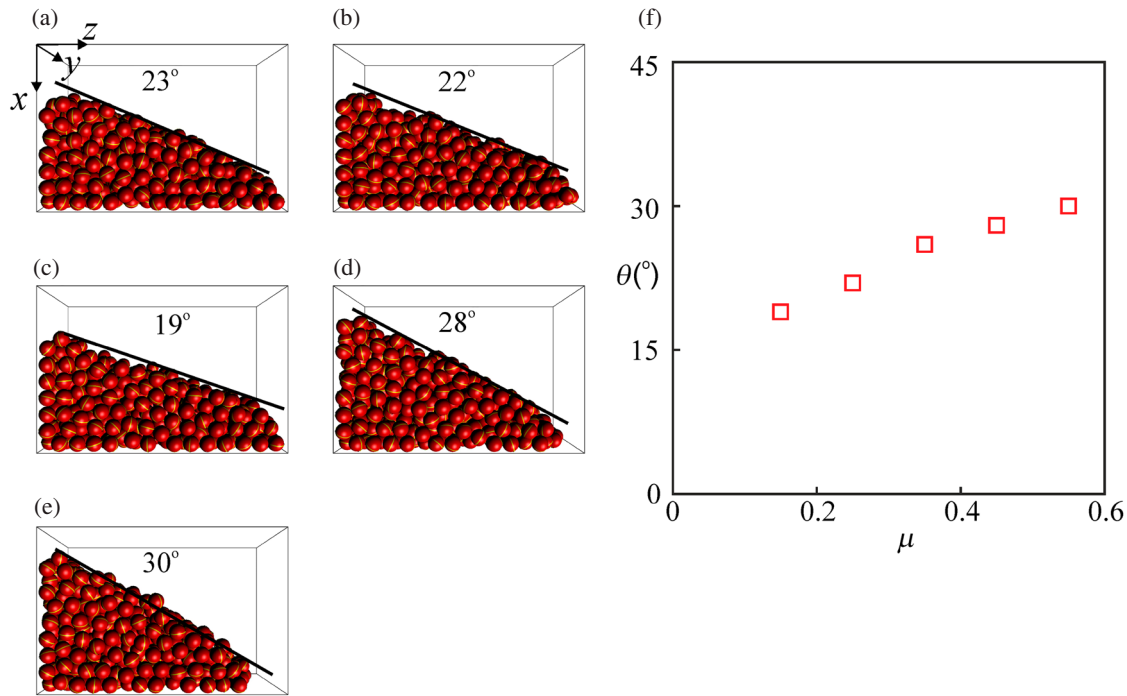


Figure 6. Simulated rest angle results. (a): $Ar_b = 5.95 \cdot 10^3$ and $\mu = 0.25$; (b–e) $Ar_b = 1.46 \cdot 10^3$ and $\mu = 0.25, 0.15, 0.45$ and 0.55 respectively; (f) rest angle θ as a function of friction coefficient μ for $Ar_b = 1.46 \cdot 10^3$.

the angle of repose in the simulations is not that sensitive for the viscosity. The angle does depend on μ . For $\mu = 0.45$ the angle of repose is to a fair approximation 28° (which is close to the experimental cases), and this is the value of the friction coefficient used in the subsequent alien particle penetration simulations.

3.3. Summary of the simulation approach

The fluid flow is solved on a uniform, cubic grid with the lattice-Boltzmann method with explicit time stepping. The granular bed consists of equally sized solid spheres. An immersed boundary method imposes no-slip at the solid particle surfaces. It also provides the hydrodynamic forces and torques on each particle. Along with short-range particle–particle interaction forces this allows updating of the particle locations and orientation (with the same time step as the flow solver) as well as their linear and angular velocities. The short-range interaction forces are lubrication forces, that compensate for a lack of resolution of the flow solver upon closely spaced solid surfaces, and “dry” collision forces. As part of the latter, the friction coefficient has been calibrated through separate simulations where the rest angle is calculated and compared with experimental data.

4. Experimental results

4.1. Effects of orientation, length and density of the alien particle

We start the analysis of the experimental results with focusing on how steel cylinders penetrate the granular

bed that contains mixture #5 as the liquid phase. Figure 7 compares the intrusion process between a cylinder entering the bed horizontally and vertically. Based on the distances the cylinder travels between image frames we estimate the speed of the cylinder just before its first contact with the granular bed as $|\mathbf{u}_{ai}| = 0.311 \text{ m s}^{-1}$ for the horizontal cylinder and $|\mathbf{u}_{ai}| = 0.314 \text{ m s}^{-1}$ for the vertical cylinder. In horizontal orientation this relatively long ($\ell/d_a = 3$), the cylinder experiences more drag than in vertical orientation. However, the distance travelled before hitting the granular bed is larger for the horizontal cylinder ($h - d_a/2 = 28 \text{ mm}$) than for the vertical one ($h - \ell/2 = 24 \text{ mm}$). The impact speeds give rise to impact Reynolds numbers $Re_{ci} = |\mathbf{u}_{ai}|d_a/\nu \approx 320$ for horizontal as well as for vertical orientation. These values along with the short settling distance imply laminar flow conditions. The camera frames do not show evidence of a “splash” of bed particles upon impact of the alien particle on the bed.

Higher drag while moving through the liquid but also through the particle bed leads to lower immersion depths for horizontal cylinders as compared to vertical ones, at least if $\ell/d_a \geq 2$ (Figure 8). Dimensionless immersion depth is defined as $s/d_b = (z_{bs} - z_{a\infty})/d_b$ with z_{bs} the vertical location of the undisturbed bed surface and $z_{a\infty}$ the eventual ($t \rightarrow \infty$) vertical location of the centre of the alien particle. Higher values of ℓ/d_a lead to higher immersion depth simply because of a larger mass of the alien particle if it is longer.

In Figure 9 we further investigate the effect of the mass of a vertically released alien particle on its

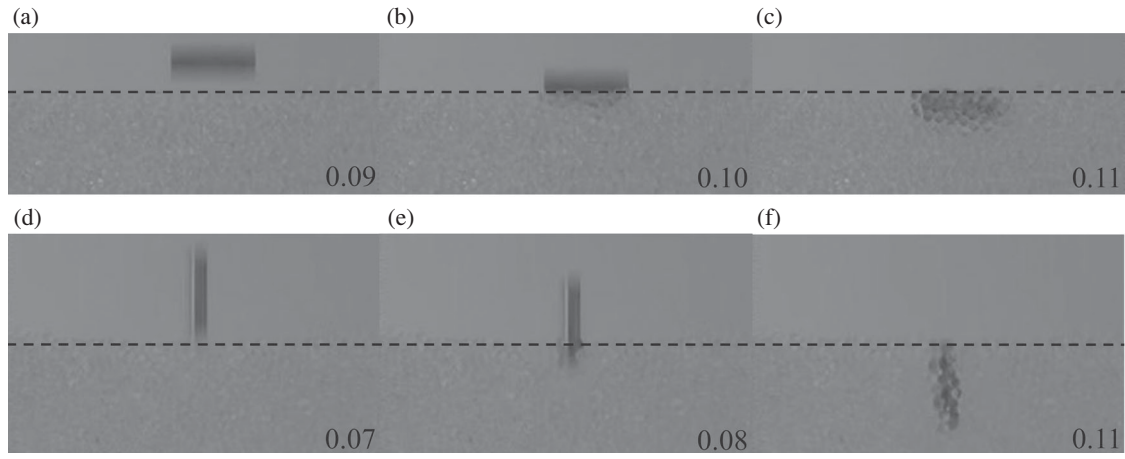


Figure 7. Camera frames of a stainless steel cylinder of length $\ell = 12$ mm and diameter of $d_a = 4$ mm intruding in a granular bed having an interstitial liquid with viscosity of $\eta = 4.28$ mPa s (mixture #5). (a–c) horizontal release; (d–f) vertical release. The frames show pre-immersion, partial immersion and full immersion respectively. Dimensionless time tv/d_b^2 has been indicated for each panel. The dashed lines indicate the granular bed surface.

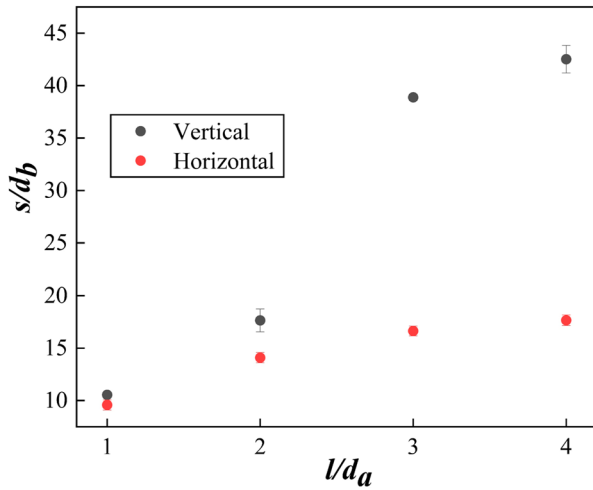


Figure 8. Depth of penetration $s = z_{bs} - z_{a\infty}$ for stainless steel cylinders in a granular bed containing liquid with a viscosity of $\eta = 4.28$ mPa s (mixture #5) as a function of the length ℓ of the cylinder. Comparison between vertical and horizontal cylinder orientation. The error bars show one standard deviation on either side based on three repeated experiments.

penetration depth. The mass is varied in two ways: by varying the alien particle density and by changing the cylinder's length while keeping its diameter the same. We expect the penetration depth to increase with net gravity on the intruder which is proportional to $(\gamma_a - 1)d_a^3\ell/d_a$ and decrease with the area with which the intruder hits the granular bed which is proportional to d_a^2 . If, as an ansatz, we assume these relations to be linear then $s \propto (\gamma_a - 1)d_a^3(\ell/d_a)/d_a^2$. With no variation in d_a and in d_b in the experiment we get $s/d_b \propto (\gamma_a - 1)\ell/d_a$. This is, to a fair approximation, what we see in Figure 9, at least for $(\gamma_a - 1)\ell/d_a < 15$. The superlinear behaviour beyond 15 might be due to the inertial mass of the alien particle, which was not part of the above analysis.

The data points in Figures 8 and 9 all have error bars that are based on repeated experiments. As noted in

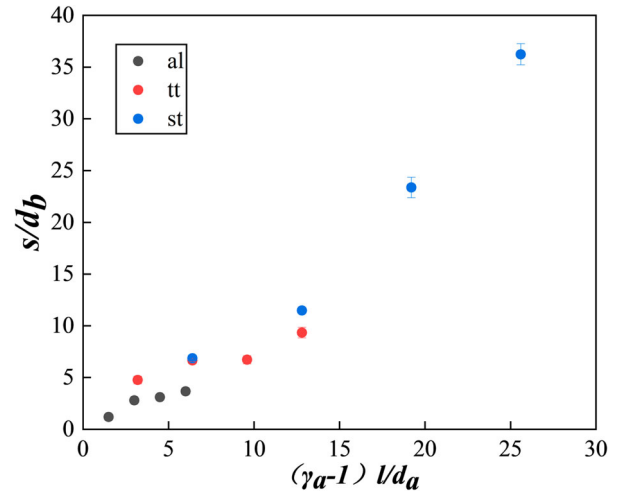


Figure 9. Depth of penetration as a function of $(\gamma_a - 1)\ell/d_a$ to test net gravity scaling. All cylinders (al = aluminium, tt = titanium, st = steel) have a $d_a = 4$ mm diameter and settle vertically. The interstitial liquid has a viscosity of $\eta = 3.14$ mPa s (mixture #4).

the context of Figure 3 and Table 3, Figures 8 and 9 also demonstrate that the experiments have good reproducibility.

4.2. Effect of the viscosity of the interstitial liquid

It is intriguing to see how the intrusion process depends on the viscosity of the interstitial liquid in the granular bed, as we show in Figures 10–12. In the experiments, the results of which are in Figure 10, the same steel cylinder with $\ell/d_a = 3$ is dropped from the same height above the granular bed surface through liquids with different viscosity. The overall trend is that immersion depth increases with increasing viscosity (the only exception of this trend is for the second data point). It is difficult to explain this trend. At first sight one might expect the opposite trend – lower viscosity leading to deeper penetration – to appear. The rationale

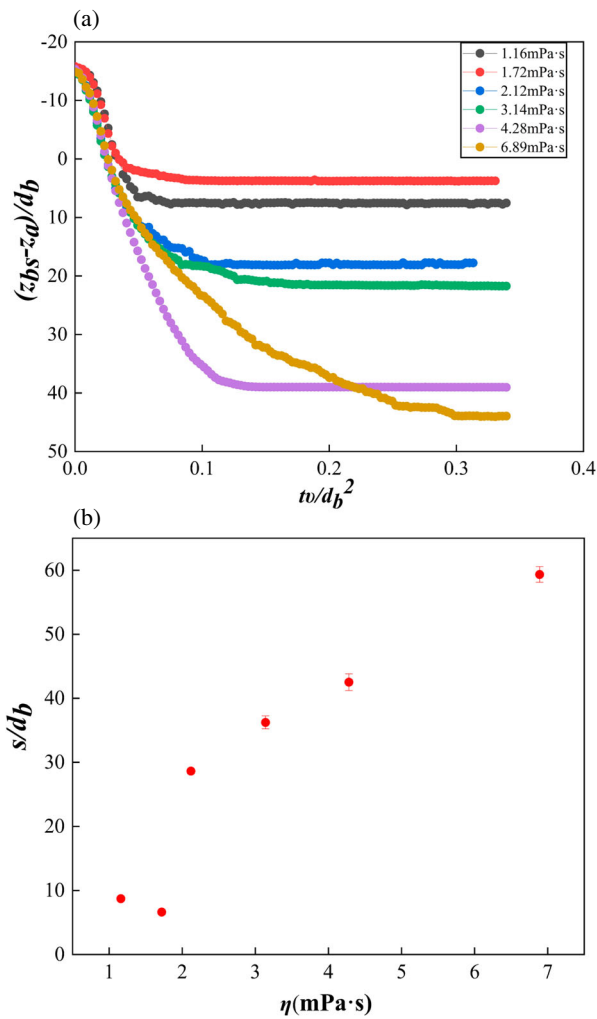


Figure 10. (a) Time series of the vertical location of a stainless steel cylinder ($d_a = 4$ mm, $\ell = 12$ mm) in a granular bed containing liquid of different viscosities. (b) Eventual depth of immersion as a function of the viscosity.

behind such an expectation would be that for the alien particle to immerse itself in the granular bed it needs to separate some of the initially closely spaced bed particles which is harder to do with a more viscous interstitial liquid. Given the experimental results, this effect, if it is actually present, is more than compensated for by (an)other effect(s) working in the opposite direction.

One mechanism that could account for such effects in the opposite direction is that the way the granular bed is packed depends on the viscosity, or, more precisely, on the bed-Archimedes number $Ar_b = (\gamma - 1)gd_b^3/\nu^2$. As an example, at larger bed solids density (larger γ) a sedimented bed might have packed more firmly, and therefore becomes less “flowable”, compared to a bed consisting of lighter particles. That is, if Ar_b increases (in this example as a result of a larger γ) the bed gets more firm and thus less penetrable. One other way to increase Ar_b is to decrease the kinematic viscosity ν which, again, could make the bed less flowable. Figure 11 shows more evidence of a less penetrable bed for lower liquid viscosity. It is important

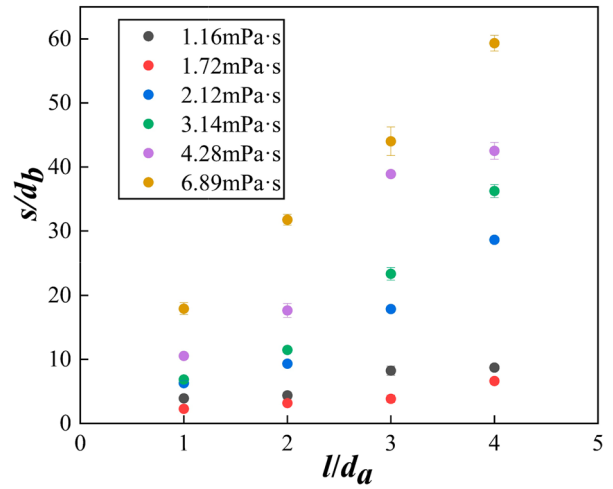


Figure 11. Depth of penetration as a function of cylinder length for stainless steel cylinders of $d_a = 4$ mm in diameter and vertical orientation. Comparison between different liquid viscosities.

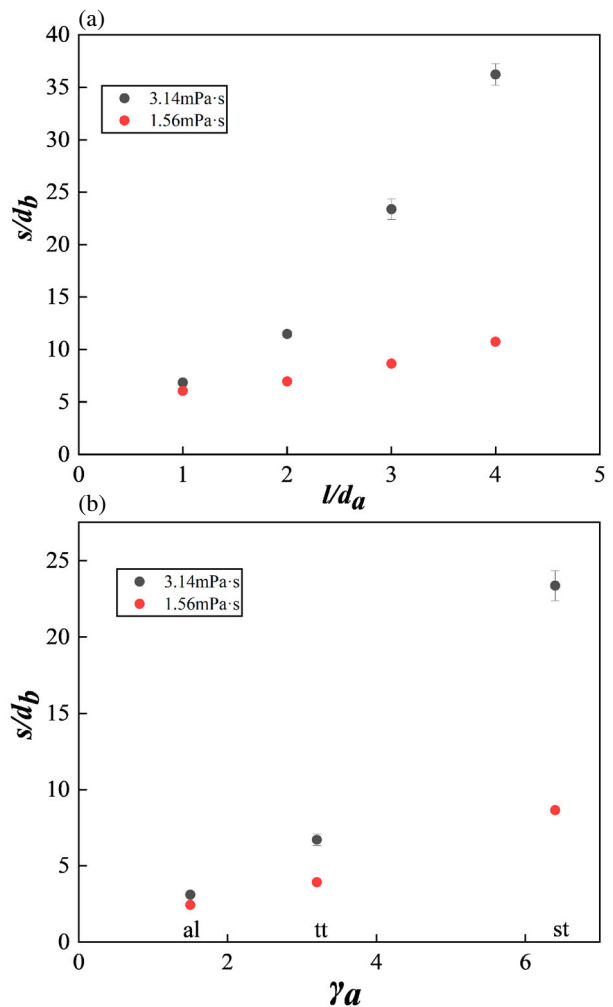


Figure 12. Comparison between liquids with the same density of $\rho = 1080$ kg m $^{-3}$ but different viscosity ($\eta = 1.56$ mPa s, and $\eta = 3.14$ mPa s; mixtures #4 and #7 respectively). (a) Immersion depth of vertical stainless steel cylinders of $d_a = 4$ mm as a function of their length. (b) Immersion depth of vertical cylinders of $d_a = 4$ mm and $\ell = 12$ mm as a function of their density ratio $\gamma_a = \rho_a/\rho$ (al = aluminium, tt = titanium, st = steel).

to note that we have no experimental evidence that the solids volume fraction of the bed depends on the viscosity.

We note that in the results presented in Figures 10 and 11 not only is the viscosity of the liquids changing, but also the density is slightly different (Table 1). To rule out a possible influence of liquid density on our penetration results we made two liquids with the same density of 1080 kg m^{-3} but viscosities that differ by a factor of two (mixture #4 has $\eta = 3.14 \text{ mPa s}$; mixture #7 is a sodium-chloride in water solution that has $\eta = 1.56 \text{ mPa s}$). Results for the penetration depth in beds with these two liquids are in Figure 12 (including the effects of cylinder length as well as the effect of cylinder density); all showing deeper penetration for the more viscous liquid. As shown in Figure 4 and Table 1, the bed with mixture #7 also has a slightly lower angle of repose and thus somewhat lower friction. Still, the alien particles penetrates (much) less deep than in the bed with mixture #4. We will use the data in Figure 12b for assessing the results of our simulations.

5. Simulation results and comparison with experiment

As discussed above, it is unpractical to simulate the experimental system in full given its large number of granular bed particles ($\sim 5 \times 10^4$). We will present results for three granular beds. One bed (*wd* – wide domain) has a footprint $L_x \times L_y = 16d_b \times 10d_b$, it contains 2880 bed particles that come to a level of $z_{bs} \approx 17.5d_b$. As we will see, this bed is too shallow to accommodate the steel cylinder. The second bed which is taller (*td* – tall domain). It contains 2400 bed particles and has $L_x \times L_y = 10d_b \times 10d_b$ and $z_{bs} \approx 23.5d_b$.

These two beds gave reasonable results for the lighter alien particles but less so for the steel particle. A third granular bed (*twd* – tall & wide domain) was created with $L_x \times L_y = 16d_b \times 10d_b$, $z_{bs} \approx 23.2d_b$ and a number of bed particles of 3840.

We will be probing two viscosities in the simulations. In light of what we wrote above about the possible effect of the bed structure on the liquid viscosity it is important to state here that the granular beds were created for the different liquids separately. The heights of the beds for the two viscosities were the same within $0.06d_b$, which translates to a difference in solids volume fraction of ~ 0.002 .

In Figure 13 we show impressions of a simulation with the wide domain and with a steel cylinder that has diameter $d_a = 2d_b$ and $\ell/d_a = 3$. The bed Archimedes number Ar_b is such that it corresponds to mixture #4 in the experiment. After vertical release the cylinder accelerates under gravity and hits the bed surface at an impact Reynolds number of $Re_i = |\mathbf{u}_{ai}|d_a/\nu = 460$. While penetrating the bed it creates a significant flow of interstitial liquid in the bed. The flow makes itself known over the full width (L_x) of the domain (Figure 13b) so that effects of the side walls might be present; the same is true for the front and back wall (Figure 13c). After a dimensionless time of $tv/d_b^2 \approx 0.3$ (this would correspond to 0.5 s in the experiment) the cylinder comes to a halt with its centre at a depth of approximately $10d_b$ (Figure 13e).

The experiments have shown that in most cases an increasing viscosity of the interstitial liquid leads to an increased penetration depth. The experimental results of Figure 10b – which clearly show this viscosity effect – have been used to design and run a series simulations, the results of which are in Figure 14. It shows the

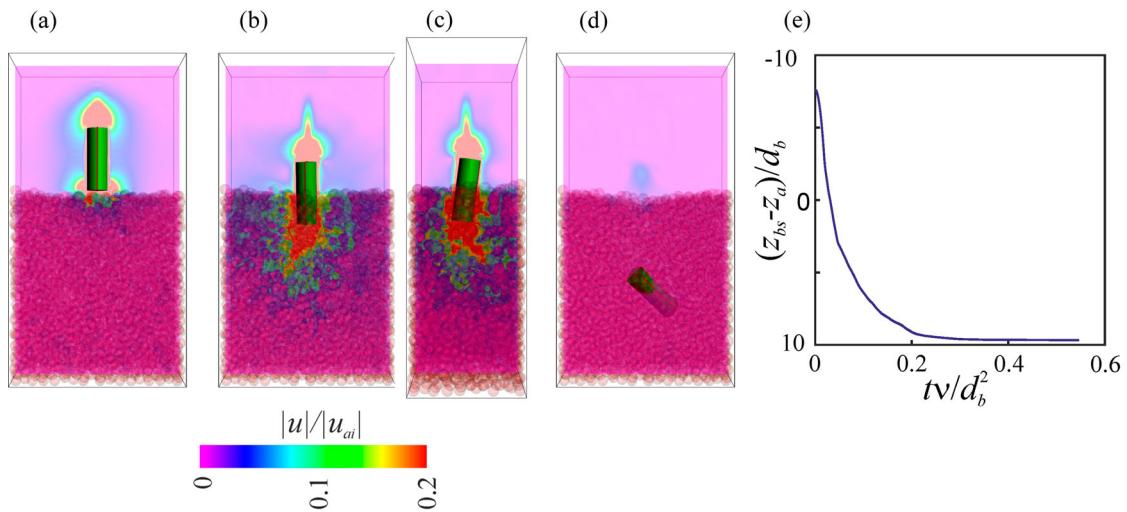


Figure 13. Simulation of a vertical cylinder with $\ell/d_a = 3$, $d_a/d_b = 2$, $\gamma_a = 7.3$ (steel), $h/d_b = 7.5$ and $Ar_b = 1.46 \cdot 10^3$. The size of the computational domain is $(L_x \times L_y \times L_z)/d_b^3 = 16 \times 10 \times 30$. (a) $tv/d_b^2 = 0.0178$; (b) $tv/d_b^2 = 0.0301$; (c) $tv/d_b^2 = 0.0301$ side view; (d) $tv/d_b^2 = 0.383$. The colours indicate the liquid velocity magnitude in the mid-planes with \mathbf{u}_{ai} the vertical velocity of the cylinder at impact. The bed particles have been made partially transparent so as to be able to see the intruder. (e) Time series of the intrusion depth of the cylinder.

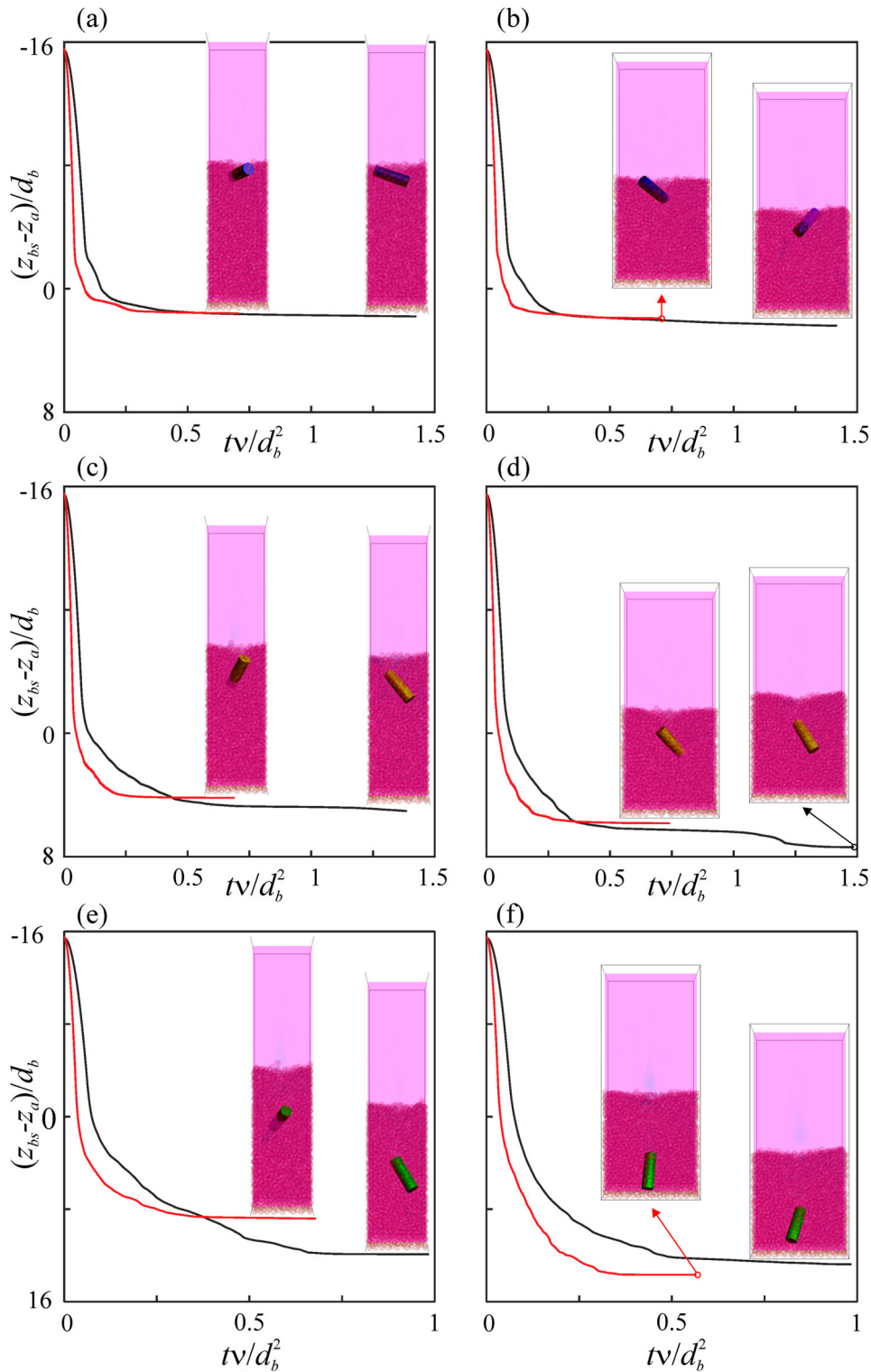


Figure 14. Simulated time series of the vertical position of vertically intruding cylinders with $\ell/d_a = 3$ and $d_a/d_b = 2$. From top to bottom: aluminium ($\gamma_a = 2.5$), titanium ($\gamma_a = 4.2$) and steel ($\gamma_a = 7.3$). Left: tall domain ($(L_x \times L_y \times L_z)/d_b^3 = 10 \times 10 \times 44$); right: wide domain ($(L_x \times L_y \times L_z)/d_b^3 = 16 \times 10 \times 38$). Black curves: high viscosity ($Ar_b = 1.46 \cdot 10^3$); red curves: low viscosity ($Ar_b = 5.95 \cdot 10^3$). Release height $h/d_b = 15$. The insets show the bed and intruder at the end of each time series.

penetration – in the form of time series and end-states – of three cylinders (aluminium, titanium and steel), all with $\ell/d_a = 3$, for two viscosities/bed-Archimedes numbers in two computational domains (wd and td) defined above. In dimensionless form the low viscosity time series (red curves) are shorter than the high viscosity ones (black curves); in real time they approximately have the same length.

To begin with, increased cylinder mass as a result of higher solid density leads to deeper penetration in the granular bed, and in the simulations. The “viscosity effect” is also observed in most cases. For the aluminium cylinder the effect is marginal in both domains investigated. For the titanium cylinders it is much clearer; it is also important to note that in the more viscous liquid the cylinder keeps (very) slowly sinking

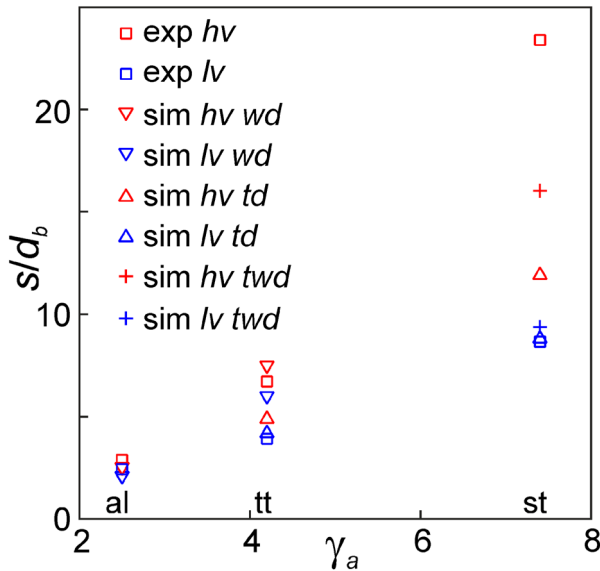


Figure 15. Eventual immersion depth $s = z_{bs} - z_{a\infty}$ as function of the alien particle density over liquid density ratio γ_a (al = aluminium, tt = titanium, st = steel). Experimental data for high viscosity (hv) and low viscosity (lv) and simulation data for high and low viscosity and a wide domain (wd), a tall domain (td) and a wide & tall domain (twd) as defined in the text.

for a long time; much longer than in the less viscous liquid where the cylinder reaches a truly zero-velocity state much sooner. For the steel cylinder the simulation results are less clear, partly because of perceived effects of domain size. In the wide domain it sinks deeper in the less viscous liquid, contrary to the experimental evidence. One can see, however, that one end of the steel cylinder has almost reached the bottom of the container in both (low and high viscosity) cases. In the tall domain (lower left panel of Figure 14) the eventual locations are well above the bottom and then the cylinder gets deeper in the bed with the more viscous liquid.

The simulations have been designed such that the results can be directly compared with the experimental data of Figure 10b. We show this comparison in Figure 15 where we have left out the steel-wide-domain simulation data given insufficient depth of the bed, and the aluminium-tall-domain data given their overlap with the other data points for aluminium. The issue that directly catches the eye in Figure 15 is the penetration of the steel cylinder in the high viscosity bed that is severely underestimated by the simulations (well outside the uncertainty range of the experiments; Figure 10b), while the penetration depth in the low viscosity bed matches the experiments. The additional simulations in the larger domain (twd) again demonstrate the effect of domain size for the high viscosity system. Where the penetration depth for the low viscosity system is very close to the one in the td, it strongly increases for the high viscosity and thus gets closer to the experimental results.

The other simulation data points follow the right trends and are quantitatively reasonable.

6. Discussion and conclusions

Results of experiments and simulations on cylindrical particles penetrating liquid-saturated granular beds have been presented. The granular bed is well-defined, it consists of mono-sized spheres in Newtonian liquid and can be largely characterized by an Archimedes number $Ar_b = (\gamma - 1)gd_b^3/\nu^2$, a solids volume fraction and an angle of repose, the latter representing the friction between the spheres. It was experimentally found that the angle of repose is mostly independent of the liquid properties.

The penetration of the alien cylindrical particles in the bed is a well reproducible process as observed in terms of the vertical location as a function of time and in terms of the eventual depth of penetration. This is remarkable given that the diameter of the alien particle is only two times that of the bed spheres so that, at least for a vertically oriented cylinder, on impact with the bed it directly interacts only with a few bed particles that are, by the nature of the granular bed, located randomly. It has been reported in this paper how the penetration depth depends on the density of the cylinder material, on the length-over-diameter aspect ratio of the cylinder, and on the orientation (vertical versus horizontal) of the cylinder. However, the most interesting dependency is that on the viscosity of the interstitial liquid of the bed with mostly larger penetration depths for higher viscosities. Given that in dimensionless terms the bed can be characterized by Ar_b , the solids volume fraction and the friction between the bed particles (i.e. a friction coefficient μ), and that the latter two do not significantly depend on the viscosity, this implies that the penetration depth depends on Ar_b , with higher Ar_b leading to less penetration. For now the underlying physical mechanisms of this dependency remain unclear.

Particle-resolved simulations were designed to try and reproduce a subset of the experimental results, focusing on the viscosity effect. The size of the experimental bed is a challenge for the simulations so that, for now, relatively small granular beds were considered. We took care, however, to have the same size of the bed in the depth direction as in the experiments so that effect of the front and back wall of the container were, in principle, captured. The simulations do show the viscosity effect. The extent of the effect is, however, much smaller than in the experiment for the heavier (steel) cylinders.

The fact that the simulations reproduce the effect of viscosity to some extent is an avenue for further research on its underlying physics given the wealth of information contained in the simulation results (such as bed topology, force and torque interactions between

particles, tracks of particle motion, the distribution of bed particle coordination numbers). In this respect it will be beneficial to first increase the domain size of the simulations which, to start with, will require an effort in improving computational efficiency.

On the experimental side it will be relevant to further explore if the viscosity effect indeed is a bed-Archimedes number effect. This can be done by changing the Archimedes number through changing parameters, other than the viscosity, that constitute this number, such as bed particle diameter or bed particle density (changing gravitational acceleration might prove too challenging experimentally).

Acknowledgements

The authors gratefully acknowledge the support of Drs Zhipeng Li and Chao Wang of Beijing University of Chemical Technology (BUCT) for making available their image analysis software and for tailoring it to our specific application.

Disclosure statement

No potential conflict of interest was reported by the author(s).

Funding

This work was supported by the National Natural Science Foundation of China [grant numbers: 22078191, 21978165, 22081340412 and 92156020].

Data availability statement

Data will be made available on request.

Notation

Ar_b	Archimedes number of the granular bed (–)
d_a	alien cylinder diameter (m)
d_b	granular bed particle diameter (m)
e	restitution coefficient (–)
g	gravitational acceleration (m s^{-2})
H	vertical domain size for bed settling simulation (m)
h	drop height (m)
k	spring stiffness for particle-particle collisions (N m^{-1})
L_x, L_y, L_z	dimensions of flow domain (m)
ℓ	length of alien cylinder (m)
Re_i	Reynolds number at impact (–)
s	immersion depth (m)
t	time (s)
\mathbf{u}	fluid velocity (m s^{-1})
\mathbf{u}_{ai}	alien particle velocity at impact (m s^{-1})
x, y, z	Cartesian coordinates (m)
$z_{a\infty}, z_a, z_{bs}$	(eventual) vertical location of centre of alien particle and of granular bed surface (m)

γ_a, γ	alien particle and bed particle density over liquid density (–)
Δ	lattice spacing (m)
Δt	time step (s)
δ_s, δ_l	activation distance for spring force and lubrication force (m)
η	dynamic viscosity (Pa s)
θ	rest angle ($^\circ$)
μ	friction coefficient (–)
ν	kinematic viscosity ($\text{m}^2 \text{s}^{-1}$)
ρ, ρ_a, ρ_b	liquid, alien particle and bed particle density (kg m^{-3})
ϕ	solids volume fraction (–)

ORCID

Lijuan Zhang  <http://orcid.org/0000-0001-5598-8691>

Jos J. Derksen  <http://orcid.org/0000-0002-9813-356X>

References

- Derksen, J. J. (2019). Liquid fluidization with cylindrical particles: Highly resolved simulations. *AIChE Journal*, 65(6), e16594. <https://doi.org/10.1002/aic.16594>
- Derksen, J. J. (2022). Settling of heavy cylindrical particles in granular beds. *International Journal of Multiphase Flow*, 157, 104232. <https://doi.org/10.1016/j.ijmultiphaseflow.2022.104232>
- Donev, A., Cisse, I., Sachs, D., Variano, E. A., Stillinger, F. H., Connelly, R., Torquato, S., & Chaikin, P. M. (2004). Improving the Density of Jammed Disordered Packings Using Ellipsoids. *Science*, 303(5660), 990–993. <https://doi.org/10.1126/science.1093010>
- Eggels, J. G. M., & Somers, J. A. (1995). Numerical simulation of free convective flow using the lattice-Boltzmann scheme. *International Journal of Heat and fluid flow*, 16(5), 357–364. [https://doi.org/10.1016/0142-727X\(95\)00052-R](https://doi.org/10.1016/0142-727X(95)00052-R)
- Garcia, M. H. (Ed.). (2008). *Sedimentation Engineering: Theories, Measurements, Modeling, and Practice*. American Society of Civil Engineers. <https://doi.org/10.1061/9780784408148>
- Goldstein, H., Poole, C. P. J., Safko, J. L., & Addison, S. R. J. A. J. o. P. (2002). *Classical Mechanics*. Pearson. <https://doi.org/10.1119/1.1484149>
- Kamrin, K., Hill, K. M., Goldman, D. I., & Andrade, J. E. (2024). Advances in Modeling Dense Granular Media. *Annual Review of Fluid Mechanics*, 56(1), 215–240. <https://doi.org/10.1146/annurev-fluid-121021-022045>
- Krüger, T., Kusumaatmaja, H., Kuzmin, A., Shardt, O., Silva, G., & Viggien, E. M. J. S. I. P. (2017). *The lattice Boltzmann method : Principles and Practice*. Springer Cham. <https://doi.org/10.1007/978-3-319-44649-3>
- Kuipers, J. B. (2020). *Quaternions and rotation sequences: A primer with applications to orbits, aerospace, and virtual reality*. Princeton university press. <https://doi.org/10.2307/j.ctvx5wc3k>
- Leiser, R., Schumann, M., Dadi, T., & Wendt-Potthoff, K. (2021). Burial of microplastics in freshwater sediments facilitated by iron-organo flocs. *Scientific Reports*, 11(1), 24072. <https://doi.org/10.1038/s41598-021-02748-4>
- Li, C., Umbanhowar, P. B., Komsuoglu, H., Koditschek, D. E., & Goldman, D. I. (2009). Sensitive dependence of the motion of a legged robot on granular media. *Proceedings of the National Academy of Sciences*, 106(9), 3029–3034. <https://doi.org/10.1073/pnas.0809095106>

- Liu, C., Tang, X., Wei, H., Wang, P., & Zhao, H. (2020). Model Tests of Jacked-Pile Penetration into Sand Using Transparent Soil and Incremental Particle Image Velocimetry. *KSCE Journal of Civil Engineering*, 24(4), 1128–1145. <https://doi.org/10.1007/s12205-020-1643-4>
- Marston, J. O., Vakarelski, I. U., & Thoroddsen, S. T. (2012). Sphere impact and penetration into wet sand. *Physical Review E*, 86(2), 020301. <https://doi.org/10.1103/PhysRevE.86.020301>
- Nelson, E. L., Katsuragi, H., Mayor, P., & Durian, D. J. (2008). Projectile Interactions in Granular Impact Cratering. *Physical Review Letters*, 101(6), 068001. <https://doi.org/10.1103/PhysRevLett.101.068001>
- Somfai, E., van Hecke, M., Ellenbroek, W. G., Shundyak, K., & van Saarloos, W. (2007). Critical and noncritical jamming of frictional grains. *Physical Review E*, 75(2), 020301. <https://doi.org/10.1103/PhysRevE.75.020301>
- ten Cate, A., Nieuwstad, C. H., Derksen, J. J., & Van den Akker, H. E. A. (2002). Particle imaging velocimetry experiments and lattice-Boltzmann simulations on a single sphere settling under gravity. *Physics of Fluids*, 14(11), 4012–4025. <https://doi.org/10.1063/1.1512918>
- Torquato, S., Truskett, T. M., & Debenedetti, P. G. (2000). Is Random Close Packing of Spheres Well Defined? *Physical Review Letters*, 84(10), 2064–2067. <https://doi.org/10.1103/PhysRevLett.84.2064>
- van der Meer, D. (2017). Impact on Granular Beds. *Annual Review of Fluid Mechanics*, 49(1), 463–484. <https://doi.org/10.1146/annurev-fluid-010816-060213>
- Zuñiga, R., Job, S., & Santibanez, F. (2019). Effect of an interstitial fluid on the dynamics of three-dimensional granular media. *Physical Review E*, 99(3), 032905. <https://doi.org/10.1103/PhysRevE.99.032905>